Journal of Power Sources 194 (2009) 625–630

Contents lists available at ScienceDirect

Journal of Power Sources

journal homepage: www.elsevier.com/locate/jpowsour

Short communication

# $La_{0.84}Sr_{0.16}MnO_{3-\delta}$ cathodes impregnated with $Bi_{1.4}Er_{0.6}O_3$ for intermediate-temperature solid oxide fuel cells

Junliang Li, Shaorong Wang*, Zhenrong Wang, Renzhu Liu, Tinglian Wen, Zhaoyin Wen

*The Key Laboratory of Energy Conversion Materials, Shanghai Institute of Ceramics, Chinese Academy of Sciences, 1295 Dingxi Road, Shanghai 200050, PR China*

ARTICLE INFO

*Article history:*
Received 7 May 2009
Received in revised form 18 June 2009
Accepted 19 June 2009
Available online 30 June 2009

*Keywords:*
Intermediate-temperature solid oxide fuel cells
Composite cathode
Impedance spectroscopy
Ion-impregnation
Bismuth oxides

ABSTRACT

$La_{0.84}Sr_{0.16}MnO_{3-\delta}$–$Bi_{1.4}Er_{0.6}O_3$ (LSM–ESB) composite cathodes are fabricated by impregnating LSM electronic conducting matrix with the ion-conducting ESB for intermediate-temperature solid oxide fuel cells (IT-SOFCs). The performance of LSM–ESB cathodes is investigated at temperatures below 750 °C by AC impedance spectroscopy. The ion-impregnation of ESB significantly enhances the electrocatalytic activity of the LSM electrodes for the oxygen reduction reactions, and the ion-impregnated LSM–ESB composite cathodes show excellent performance. At 750 °C, the value of the cathode polarization resistance ($R_p$) is only 0.11 Ω cm$^2$ for an ion-impregnated LSM–ESB cathode, which also shows high stability during a period of 200 h. For the performance testing of single cells, the maximum power density is 0.74 W cm$^{-2}$ at 700 °C for a cell with the LSM–ESB cathode. The results demonstrate the ion-impregnated LSM–ESB is one of the promising cathode materials for intermediate-temperature solid oxide fuel cells.



## 1. Introduction

$La_{1-x}Sr_xMnO_{3-\delta}$ (LSM) is regarded as one of the most promising cathode materials for use in the production of high-temperature solid oxide fuel cells (SOFCs) because of its high thermal and chemical stability, relatively good compatibility with zirconia-based electrolytes [1,2]. However, the electrochemical activity of the LSM-based cathodes decreases substantially with decreasing cell operating temperatures and the cathode polarization resistance dominates the cell resistance at intermediate temperatures. Therefore, it is critical to improve the LSM cathode performance in order to improve the cell performance at intermediate temperatures. Many researchers have investigated the properties of LSM-based cathodes [3–6], and it is reported that the rate-determining step of the oxygen reduction on LSM cathodes is the adsorption and surface diffusion of oxygen. Some other researchers suggested that the charge transfer reaction is the rate-determining step for the oxygen reduction reaction on LSM cathodes. However, all of them suggested that the performance of cathodes is closely related to the length of the triple phase boundary (TPB). It is reported that the composite cathodes can availably increase the length of TPB and improve their electrochemical performance [7–9], and the addition of an oxygen ion conductor into LSM to form a composite cathode is a general method. For instance, cathode polarization resistances (area specific resistances) were 2.49 and 0.75 Ω cm$^2$ at 700 °C for a LSM–YSZ cathode and a LSM–GDC cathode, respectively, which were 25 and 7.5% of the value for the LSM polarization resistance [9]. And the superior performance of the LSM–GDC composite cathode over that of LSM–YSZ was attributed to the higher ionic conductivity as well as the higher oxygen surface exchange coefficient of GDC compared with that of YSZ.

Doped bismuth oxides have been investigated recently as possible component of composite cathodes in IT-SOFCs [10–12]. Doped bismuth oxides have high levels of oxygen ion conductivity [13–15]. For instance, $Er_2O_3$-stabilized $Bi_2O_3$ (ESB) has the highest level of oxygen ion conductivity (0.37 S cm$^{-1}$ at 973 K). In addition, the oxygen surface exchange coefficient of stabilized bismuth oxide is comparable to that of other electrolytes [16]. Thus, ESB is expected to improve the electrode performance by playing the role of GDC or YSZ in composite cathodes.

Now, a more effective ion-impregnating method has been proposed to fabricate the composite cathodes [17–20]. It is an effective way to deposit electrocatalytic oxides into the porous LSM matrix without diminishing the advantages of stability and compatibility of LSM materials with zirconia-based electrolytes. In this work, LSM–ESB composite cathodes for intermediate-temperature solid oxide fuel cells (IT-SOFCs) based on the SSZ ($(ZrO_2)_{0.89}(Sc_2O_3)_{0.05}(CeO_2)_{0.01}$) electrolytes were fabricated with a two-step fabricating process including screen-printing and ion-impregnating, and the electrochemical behavior at the cathode/electrolyte was investigated by AC impedance analyses. Besides, the performance of anode-supported single cells using LSM–ESB as cathode materials was also evaluated.

* Corresponding author. Tel.: +86 21 52411520; fax: +86 21 52413903.
*E-mail address:* srwang@mail.sic.ac.cn (S. Wang).

0378-7753/$ – see front matter © 2009 Elsevier B.V. All rights reserved.
doi:10.1016/j.jpowsour.2009.06.070

## 2. Experimental

The $La_{0.84}Sr_{0.16}MnO_{3-\delta}$ (LSM) powder was synthesized by autoignition of citrate–nitrate gel as reported previously [21]. $La(NO_3)_3{\cdot}6H_2O$(>99.0%), $Sr(NO_3)_2$ (>99.5%), and $Mn(NO_3)_2{\cdot}4H_2O$ (>99.0%) in stoichiometric proportions were mixed together in a water-bath at 80 °C. When they were dissolved completely, a certain amount of citric acid was introduced to form the LSM precursor solution. The solution was heated on a hot plate till autoignition occurred, resulting in a black powder. Then the powder was sintered in air at 850 °C for 5 h to form the expected perovskite phase.

To prepare the cathode, LSM was mixed with an appropriate amount of graphite (30 wt.%) and ball-milled for 24 h to form a uniform electrode powder. Using the screen-printing method, the LSM electrode precursor was printed to the SSZ ($(ZrO_2)_{0.89}(Sc_2O_3)_{0.05}(CeO_2)_{0.01}$) substrates and then sintered at 1200 °C for 2 h in air to form porous LSM frames. The ESB particles were coated onto the inner surface of the porous LSM frames with an ion-impregnation process. An aqueous solution containing $Er(NO_3)_3$ and $Bi(NO_3)_3$ ($Er^{3+}$:$Bi^{3+}$ = 3:7) was dropped onto the top of the LSM frame, dried at room temperature, and heated at 700 °C for 2 h to form $Bi_{1.4}Er_{0.6}O_3$ (ESB) particles. The mass of the electrode before and after the impregnation treatment was measured to determine the impregnated oxide loadings. The procedure was repeated to increase the ESB loadings. The impregnated ESB loadings in LSM–ESB composite cathodes were 30, 40, 50 and 60 wt.% (named LSM–ESB30, LSM–ESB40, LSM–ESB50 and LSM–ESB60, respectively).

The polarization resistance was measured by two-electrode impedance method using symmetric cells, using an AC impedance spectroscopy (ZAHNER IM6e) with a 20 mV AC signal, over a frequency range of 0.05 Hz to 1 MHz. The area of every cathode was 1.0 $cm^2$. A three-electrode cell configuration was used to measure the overpotential of the LSM–ESB electrodes as shown in Fig. 1. A LSM–ESB working electrode was fabricated with the same process as forenamed, and the area of the working electrode was also 1.0 $cm^2$. The counter electrode was formed by applying the Pt paste to the opposite side of the working electrode on the SSZ electrolyte, and the Pt reference electrode was deposited beyond the counter electrode. Both counter and reference electrodes were fired at 800 °C for 2 h. The electrode overpotential was measured at 650 °C by a combination of EIS and DC polarization. The overpotential, $\eta$, was calculated by the following equation:

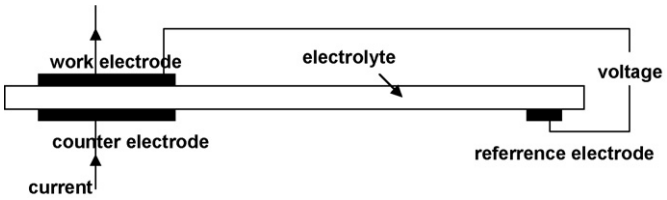


**Fig. 1.** The schematic configuration of the three-electrode cell.

$$\eta = U_{WR} - iR_{ohm}, \quad (1)$$

where $U_{WR}$ is the voltage between the working electrode and the reference electrode, obtained when passing a current, $i$, through the cell. $R_{ohm}$ is the ohmic resistance obtained from the high frequency real axis intercept of the impedance spectra. A single cell was prepared with the LSM–ESB50 composite cathode on the anode-supported SSZ film. The performance of the single cell was measured from 600 to 700 °C with humidified hydrogen (a water

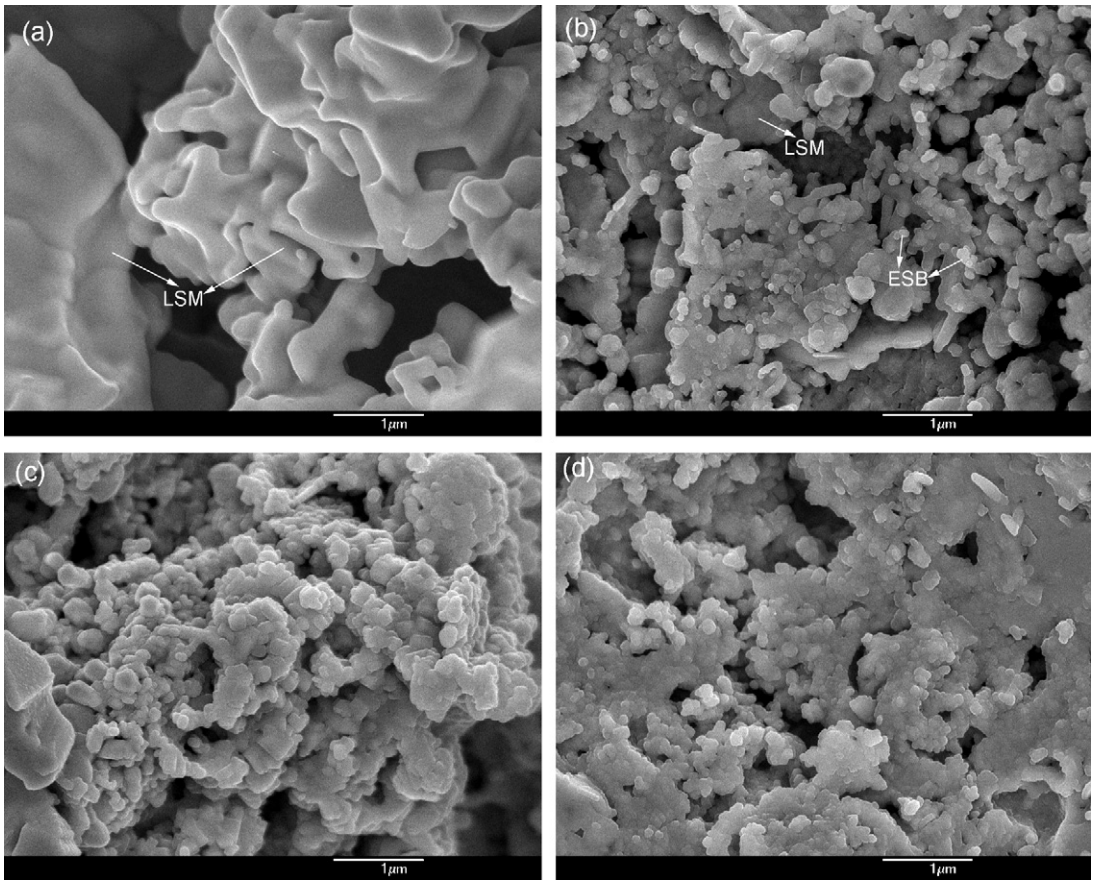


**Fig. 2.** Typical fracture cross-section SEM images of pure LSM (a), LSM–ESB40 (b), LSM–ESB50 (c) and LSM–ESB60 (d) composite cathodes.

content of around 3 vol.%) as fuel and air as oxidant. The area of the cathode was 1 $cm^2$. Ag mesh, attached to the cathode surface with Ag paste, was used as the current collector. A four-probe configuration was used for electrochemical impedance spectroscopy (EIS) measurements. Various phases of the powder were identified with a Rigaku X-ray diffraction (XRD) diffractometer at room temperature, using monochromatic Cu Kα radiation. The microstructure of the cathode section was studied by scanning electron microscopy (SEM).

## 3. Results and discussion

### 3.1. Cathode microstructure and composition

Fig. 2 shows typical cross-section SEM images of the LSM electrodes impregnated with different amounts of ESB. The pure LSM electrode is porous and consisted of LSM particles of irregular shapes (Fig. 2a), which is of great benefit for ion-impregnation. After ESB impregnation, fine spherical particles are clearly deposited in the LSM matrix. However, the distribution of the nano-sized ESB particles appears to be discrete and does not form a continuous network at low ESB loadings (Fig. 2b), which cannot provide sufficient ion transferring access. When the ESB loading increases to 50 wt.%, a continuous and porous structure of ESB is most likely formed as shown in Fig. 2c. The deposition of very fine oxygen conducting ESB particles in the LSM matrix formed a mutual surrounding structure of ionic conduction phase and electronic conduction phase, which is assumed to effectively extend the triple phase boundary (TPB) for the oxygen reduction reaction. This structure consequently leads to enhancement of the electrochemical activity and significant reduction of the cathode polarization resistance. However, when the ESB loading further increases to 60 wt.%, the ESB particles cover almost entire LSM surface and form a continuous and relatively dense layer on the inner surface of the LSM matrix (Fig. 2d), which decreases the length of TPB because oxygen cannot be transferred to the interface of ESB and LSM.

Shown in Fig. 3 are the X-ray diffraction (XRD) patterns of the LSM–ESB50 composite prepared by ion-impregnation process and finally fired at 800 °C for 20 h. XRD pattern shows that ESB was formed by ion-impregnation process. And the patterns reveal no evidence of inter-phase reactivity after heat treatment. It is concluded, therefore, that the LSM–ESB composite cathodes are stable under the experimental conditions.

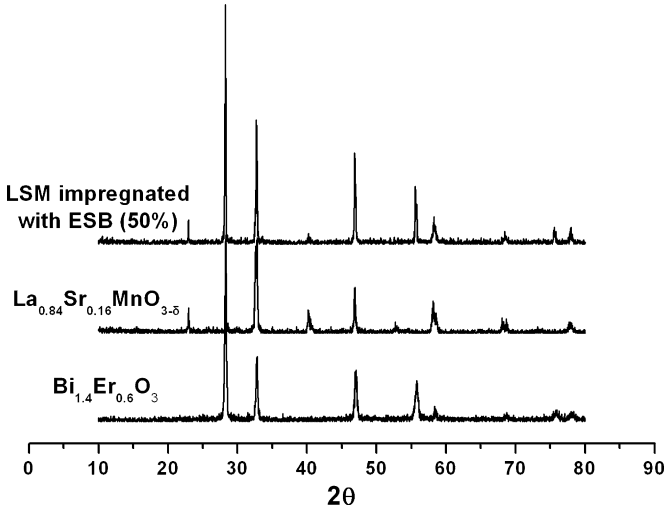


**Fig. 3.** XRD patterns of the LSM, ESB and LSM–ESB50 composite prepared by ion-impregnation process.

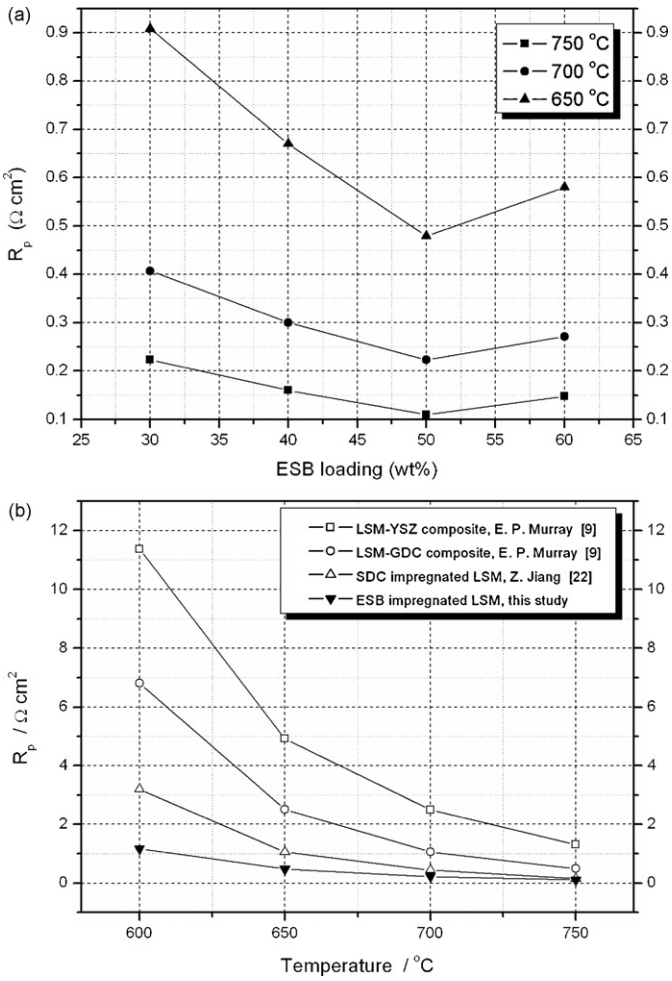


**Fig. 4.** Polarization resistances of LSM–ESB composite cathodes with various ESB loadings (a), and comparison of the resistance for LSM-based cathodes (b).

### 3.2. Effect of ESB loading

Fig. 4a shows the effect of the impregnated ESB loadings on the cathode polarization resistances ($R_p$). In general, higher loadings resulted in smaller resistances as the ESB loadings were less than 50 wt.%. The value of $R_p$, however, increased for a further increase in the ESB loadings to 60 wt.%. This may be due to a decrease in the length of TPB as forenamed and also a decrease in porosity of the LSM–ESB60 cathode, which decrease the absorption and transfer access of oxygen and lead to an increase in cathode polarization resistances. The low value of polarization resistances can be obtained only when the gas, ionic and electronic transportation phases are present at an appropriate ratio. The optimal composition, LSM–ESB50, yielded $R_p$ = 0.22 and 0.48 at 700 °C and 650 °C. Such values are about 35 times lower than those of the cathode polarization resistance for pure LSM [9]. The high performance that results from the impregnation of ESB is due to the appropriate distribution of the ESB particles in the LSM matrix, which provides the effective ionic and electronic conducting pathways and, at the same time, promotes the synergistic process involving the injection of the mobile charged oxygen species into the ionic carriers.

Shown in Fig. 4b is $R_p$ comparison for LSM-based cathodes. The performance of LSM-based electrodes is affected by both the fabrication process and the ion-conducting component that is used to increase their activity. LSM–ESB50 in this study shows relatively low $R_p$ among LSM-based cathodes including LSM–YSZ50, LSM–GDC50 (prepared by mixing) and LSM–SDC50 (prepared by

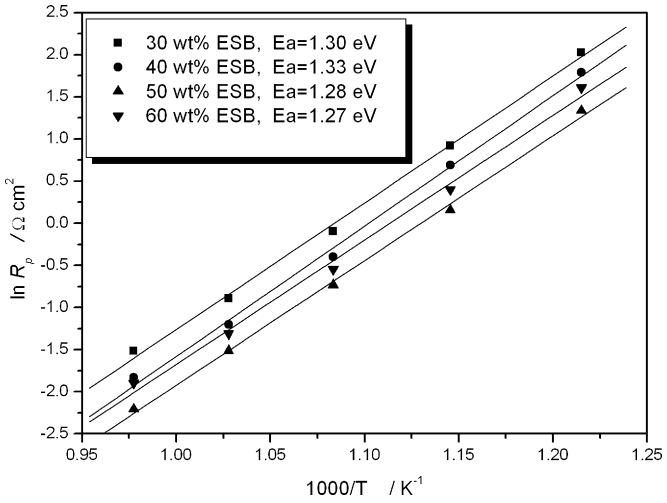


**Fig. 5.** Arrhenius plot of the polarization resistance of LSM–ESB30, LSM–ESB40, LSM–ESB50 and LSM–ESB60 cathodes.

ion-impregnation) [9,22]. In our previous study, LBSM–ESB50 and LBSM–ESB40–GDC10 also showed low $R_p$ [21,23]. For example, LBSM–ESB50 yielded $R_p$ = 0.11, 0.21, 0.39 and 1.00 Ω cm$^2$ at 750, 700, 650 and 600 °C, respectively, and LBSM–ESB40–GDC10 yielded $R_p$ = 0.09, 0.18, 0.38 and 1.17 Ω cm$^2$ at 750, 700, 650 and 600 °C, respectively. The high performance of cathodes including ESB can be explained, at least in part, by the high conductivity of ESB ($10^{-1}$ to $10^{-2}$ S cm$^{-1}$ at 700–500 °C), and the ionic conductivity is approximately one or two orders of magnitude greater than that of stabilized zirconia and ceria [24]. Meanwhile, the high conductivity of ESB allows the effective TPB to extend more deeply into the bulk of the cathode, in other words, more effective sites for oxygen reduction reactions are available. It should be also noted that bismuth oxide is a favorable catalyst for oxygen dissociation [25], which may also contribute to the high cathode performance.

Fig. 5 shows the relationship of cathode polarization resistances ($R_p$) *versus* temperatures, from which the activation energy can be calculated. The activation energy was 1.30, 1.33, 1.28 and 1.27 eV for the LSM–ESB30, LSM–ESB40, LSM–ESB50 and LSM–ESB60 electrodes, respectively. The activation energy for the LSM–ESB system is almost independent of the ESB content, suggesting that introducing ESB into the LSM cathode does not significantly change the mechanism of oxygen reduction. It is reported that the activation energy for the oxygen surface exchange reaction is around 1.25 eV [26]. The activation energy for the LSM–ESB system is similar to that of the oxygen surface exchange reaction, thus, we suggest that the rate-determining step of the electrode reaction may be attributed to an oxygen surface exchange reaction.

### 3.3. Impedance spectra for symmetrical cells

Fig. 6a–c shows impedance spectra measured in air at 700, 650, and 600 for LSM–ESB40, LSM–ESB50, and LSM–ESB60 on the SSZ electrolyte, respectively. The shape of the impedance spectra of the LSM–ESB system is similar to each other. It is noted that the impedance spectra include a high frequency arc and a dominant low frequency arc, and the arc scale depends on ESB loadings. For example, the cathode polarization resistance, $R_p$, which is the difference between the high and low frequency intercepts at the real axis, was 0.67 Ω cm$^2$ for the LSM–ESB40 cathode. It decreased to 0.48 and 0.58 Ω cm$^2$ at 650 °C for the LSM–ESB50 and LSM–ESB60 cathodes, respectively.

The different arcs in the impedance spectra correspond to different reaction steps. To identify these steps, equivalent circuit

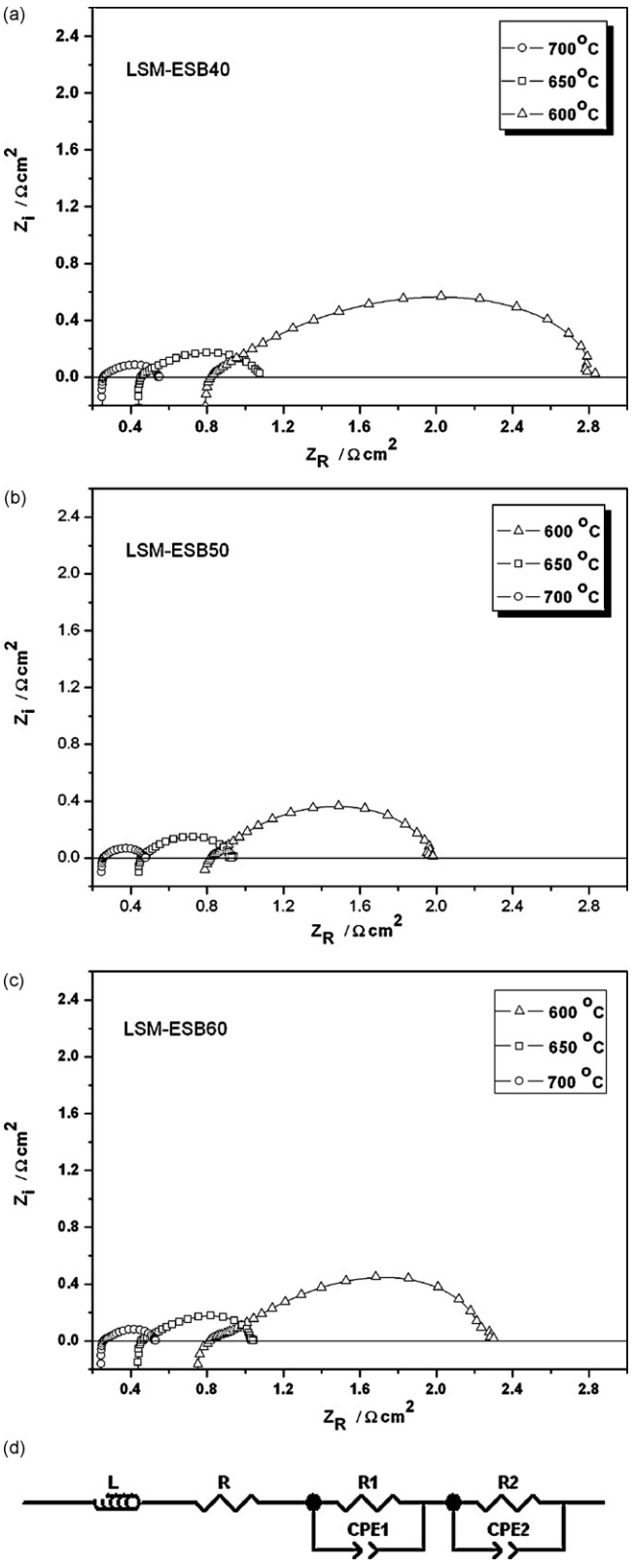


**Fig. 6.** AC impedance spectra of LSM–ESB40 (a), LSM–ESB50 (b) and LSM–ESB60 (c) cathodes measured at 600, 650 and 700 °C in air, and the corresponding equivalent circuit (d).

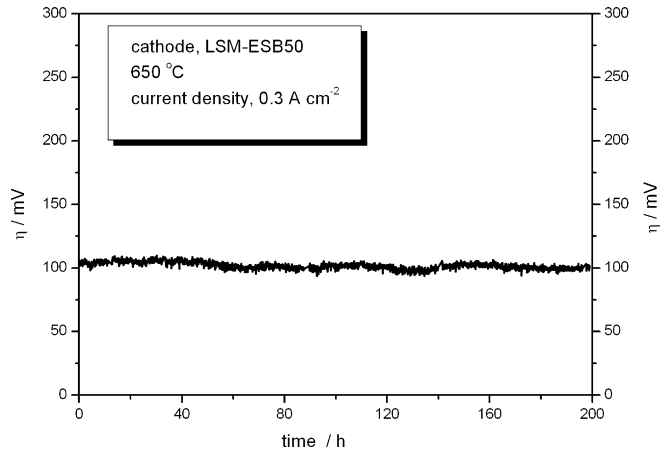


**Fig. 7.** The overpotential ($\eta$) *versus* time for the LSM–ESB50 electrode at 650 °C.

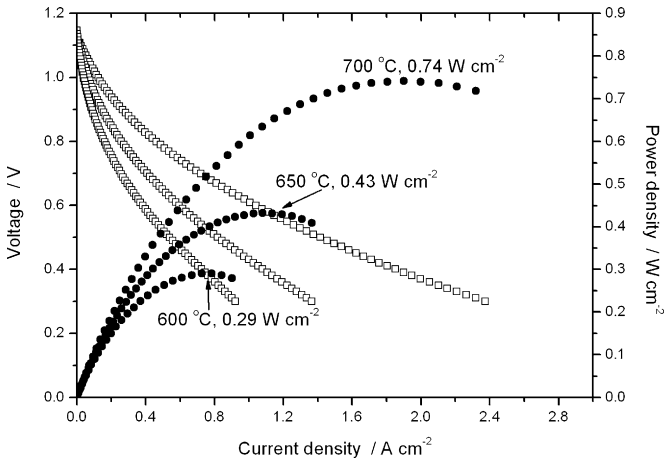


**Fig. 8.** The cell voltage and power density as a function of current density of the anode-supported single cell with the LSM–ESB50 composite cathode operating at various temperatures.

(Fig. 6d) was applied to fit the impedance spectra recorded at different temperatures using Zview program. The inductance $L$ is attributed to high-frequency artifacts arising from the measurement apparatus. $R$ corresponds to the resistance of the electrolyte and the lead wires. $R_1$ (corresponds to the relative high-frequency arc) and $R_2$ (corresponds to the relative low-frequency arc) are the corresponding polarization resistances, and CPE1 and CPE2 are the corresponding constant phase elements. Values of $R_1$ at 650 °C for LSM–ESB40, LSM–ESB50, and LSM–ESB60 cathodes were 0.1, 0.07, and 0.09 $\Omega\,cm^2$, respectively. Whereas values of $R_2$ at 650 °C were 0.57, 0.41, and 0.49 $\Omega\,cm^2$ for LSM–ESB40, LSM–ESB50, and LSM–ESB60 cathodes, respectively. The total polarization resistance ($R_p$) of the composite cathodes mainly resulted from $R_2$. It is reported that the high frequency arc usually corresponds to the incorporation of $O^{2-}$ from the TPB into the electrolyte and into the ionic conduction component in the composite cathodes, and the low frequency arc is typically attributed to the dissociative adsorption of $O_2$ [4,27]. Therefore $R_2$ is very likely to be related with the dissociative adsorption of oxygen, and we suggest that the rate-determining step of the oxygen reduction reaction on LSM–ESB system is dissociative adsorption and oxygen surface exchange reaction. The values of capacitances were $\sim 10^{-4}$ and $10^{-2}$ F for the first constant phase element (CPE1) and the second constant phase element (CPE2), respectively, and varied weakly with temperature in these composite cathodes.

### 3.4. Typical cathode stability and single cell performance

According to the investigation in this study, the LSM–ESB50 cathode showed the lowest polarization resistance in LSM–ESB system. Three-electrode cell (Fig. 1), therefore, was fabricated to study the cathode stability using LSM–ESB50 as the work electrode. As shown in Fig. 7, the overpotential, $\eta$, which was calculated by Eq. (1) as mentioned in Section 2, was almost invariable at 650 °C within 200 h and was in the range of $101 \pm 2$ mV at the current density of 0.3 A $cm^{-2}$, and it indicated that the LSM–ESB50 cathode was relatively stable within testing time.

The performance evaluation of the cell in this study was carried out by the anode-supported single cell consisting of a 700 μm-thick Ni–YSZ anode, a 15 μm-thick SSZ electrolyte, and a LSM–ESB50 cathode. The cell was measured at 600, 650 and 700 °C with humidified hydrogen (a water content of around 3 vol.%) as the fuel and air as the oxidant, and Fig. 8 shows the current voltage characteristics and the corresponding power densities for the cell. The cell produced maximum power densities of 0.29, 0.43 and 0.74 W $cm^{-2}$ at 600, 650 and 700 °C, respectively. The cell performance was higher than that of the similar cell with YSB ($Bi_{1.5}Y_{0.5}O_3$) impregnated LSM cathode, and its maximum power density was 0.20, 0.39 and 0.67 W $cm^{-2}$ at 600, 650 and 700 °C, respectively [9]. Besides, the cell performance in this study was comparable to that of the cell with the LBSM–ESB50 cathode functional layer and LBSM cathode layer, and its maximum power density was 0.25, 0.46 and 0.75 W $cm^{-2}$ at 600, 650 and 700 °C, respectively [28]. The cell performance is expected to improve by optimizing the cathode microstructure, and the results in this study demonstrate that LSM–ESB50 is a promising candidate for the cathode of IT-SOFCs.

## 4. Conclusions

The LSM–ESB cathodes on the SSZ electrolyte were fabricated using an ion-impregnating method, and their characteristics were investigated by AC impedance spectroscopy. The presence of ESB in the LSM cathode dramatically accelerated the cathode reaction and significantly reduced the cathode polarization resistance. The value of the cathode polarization resistance ($R_p$), for example, was 0.22 $\Omega\,cm^2$ at 700 °C for LSM–ESB50. Such value is about 35 times lower than that of $R_p$ for pure LSM. And the LSM–ESB50 cathode was relatively stable within testing time at 650 °C. In addition, the performance of the cell with LSM–ESB50 cathode was also measured with humidified hydrogen as the fuel and air as the oxidant. The maximum power density of the cell was 0.74 W $cm^{-2}$ at 700 °C. The results indicate that the LSM electrodes impregnated with ESB are excellent candidates as cathodes for intermediate-temperature solid oxide fuel cells.

## Acknowledgement

This work is supported financially by the Chinese High Technology Development Project (2007AA05Z151).

## References

[1] N.Q. Minh, J. Am. Ceram. Soc. 76 (1993) 563–588.
[2] B.C.H. Steele, Solid State Ionics 86–88 (1996) 1223–1234.
[3] K. Sasaki, J.P. Wurth, R. Gschwen, K. Godickemeier, L.J. Gauckler, J. Electrochem. Soc. 143 (1996) 530–543.
[4] F.H. van Heuveln, H.J.M. Bouwmeester, J. Electrochem. Soc. 144 (1997) 134–140.
[5] J. Van Herle, A.J. MacEvoy, K. Ravindranathan Thampi, Electrochim. Acta 41 (1996) 1447–1454.
[6] E. Siebert, A. Hammouche, M. Kleitz, Electrochim. Acta 40 (1995) 1741–1753.
[7] T. Kenjo, M. Nishiya, Solid State Ionics 57 (1992) 295–302.
[8] E.P. Murray, T. Tsai, S.A. Barnett, Solid State Ionics 110 (1998) 235–243.
[9] E.P. Murray, S.A. Barnett, Solid State Ionics 143 (2001) 265–273.
[10] H. Zhao, M. Pijolat, J. Mater. Chem. 12 (2002) 3787–3791.
[11] M. Camaratta, E. Wachsman, Solid State Ionics 178 (2007) 1242–1247.

[12] H.X. Hu, M.L. Liu, J. Electrochem. Soc. 143 (1996) 859–862.
[13] N.M. Sammes, G.A. Tompsett, H. NaÈ fe, F. Aldinger, J. Eur. Ceram. Soc. 19 (1999) 1801–1826.
[14] J.R. Jurado, C. Moure, P. Duran, N. Valverde, Solid State Ionics 28 (1988) 518–523.
[15] M.J. Verkerk, A.J. Burggraaf, J. Electrochem. Soc. 128 (1981) 75–82.
[16] B.C.H. Steele, Solid State Ionics 75 (1995) 157–165.
[17] S.P. Jiang, Y.J. Leng, S.H. Chan, K.A. Khor, Electrochem. Solid State Lett. 6 (2003) A67–A70.
[18] S.P. Jiang, W. Wang, Solid State Ionics 176 (2005) 1351–1357.
[19] S.P. Yoon, J. Han, S.W. Nam, T.-H. Lim, I.H. Oh, S.-A. Hong, Y.-S. Yoo, H.C. Lim, J. Power Sources 106 (2002) 160–166.
[20] X.Y. Xu, Z.Y. Jiang, X. Fan, C.R. Xia, Solid State Ionics 177 (2006) 2113–2117.
[21] J.L. Li, S.R. Wang, Z.R. Wang, R.Z. Liu, T.L. Wen, Z.Y. Wen, J. Power Sources 179 (2008) 474–480.
[22] Z. Jiang, L. Zhang, L. Cai, C. Xia, Electrochim. Acta 54 (2009) 3059–3065.
[23] J.L. Li, S.R. Wang, X.F. Sun, R.Z. Liu, X.F. Ye, Z.Y. Wen, J. Power Sources 185 (2008) 649–655.
[24] V.V. Kharton, F.M.B. Marques, A. Atkinson, Solid State Ionics 174 (2004) 135–149.
[25] Z. Jiang, L. Zhang, K. Feng, C. Xia, J. Power Sources 185 (2008) 40–48.
[26] S. Lee, Y. Lim, E.A. Lee, H.J. Hwang, J.W. Moon, J. Power Sources 157 (2006) 848–854.
[27] M.J. Jorgensen, M. Mogensen, J. Electrochem. Soc. 148 (2001) A433–A442.
[28] J.L. Li, S.R. Wang, Z.R. Wang, J.Q. Qian, R.Z. Liu, T.L. Wen, Z.Y. Wen, J. Solid State Electrochem., doi:10.1007/s10008-009-0813-6.